Majlesi Journal of Electrical Engineering **Vol. 14, No. 1, March 2020**

Backstepping Predictive Direct Power Control of Grid-Connected Photovoltaic System Considering Power Quality Issue

Brahim Elkhalil Youcefa[1*], Ahmed Massoum[1], Said Barkat[2], Patrice Wira[3]
1- Département of Electrotechnique, Université Djillali Liabes de Sidi Bel Abbes, Sidi Bel Abbés 22000, Algérie.
Email:khalilyoucefa@gmail.com (Corresponding author), ahmassoum@yahoo.fr
2- Laboratoire de Génie Electrique, Université de M'sila, M'sila 28000, Algérie.
said.Brakat@univ-msila.dz
3- Laboratoire IRIMAS, Université de Haute Alsace, 68093 Mulhouse, France.
Email:patrice.wira@uha.fr

Received: January 2019 Revised: April 2019 Accepted: June 2019

ABSTRACT:
In this paper, a grid connected PV system acting as shunt active power filter for power quality enhancement is presented. Further, a DC-DC boost converter is used to interface the photovoltaic generator with the grid, which provides a continuous power flow from the PV generator into the grid through a Voltage Source Inverter (VSI). Hence, a nonlinear backstepping control method with predictive direct power control for the shunt active power filter side is presented, and a suitable backstepping DC-DC boost converter is also developed, with a view to reduce harmonic currents and insuring reactive power compensation under nonlinear loads variations on the utility grid, and also extracts the maximum amount of power from the photovoltaic generator. Processor in the Loop (PIL) co-simulation results prove the performances efficiency of the implemented control algorithms under a nonlinear load operating condition.

KEYWORDS: DC-DC Boost Converter, Grid Connected PV System, Shunt Active Filter, Backstepping Control, Predictive Direct Power Control**.**

1. INTRODUCTION

The demand for electricity in the modern industrial world is rapidly increasing, from commercial industries to household utilities. Renewable energy-based distributed energy sources are becoming more attractive, on both technological and economic scales, and the integration level of this sources has been greatly increased due to several technical and environmental interests. There are different ways of harvesting energy from renewable energy sources such as Solar Photovoltaic (PV) systems which have received a great deal of attention, owing their special advantages such as simplicity in allocation, no fuel cost, and widely distributed throughout the earth [1]. Additionally, to reduce the pollution for carbon emission and environmental, the power generation from PV systems is mostly encouraged by the governments and many industries [2]. Though PV systems are suitable for both grid-connected and stand-alone modes.

The main purpose of a grid connected PV system is to transfer maximum power to the grid with a power factor close to unity. Furthermore, to avoid the additional cost of the power circuit, many research papers has investigated another function of grid connected PV system which is represented by a PV system acting as shunt active power filter for improving power quality in the utility grid [3-5]. Moreover, these systems inject active power generated by the PV to the grid and also filters the load current harmonics [6, 7]. To achieve this objective, each grid-connected PV system has to perform two essential functions; increasing the output efficiency of the PV arrays which is normally ensured through the operation of PV modules at Maximum Power Point (MPP), and inject a harmonic free sinusoidal current into the grid [8].

Nowadays, Direct Power Control (DPC) technique based on the instantaneous power theory has been introduced by H. Akagi et al. [9], this control technique is founded from the well-known Direct Torque Control (DTC) used in adjustable speed drive systems. The instantaneous active and reactive power terms is directly selected in the DPC algorithm as control variables instead of the current variables that

are commonly used in VOC system [10], which is identical to the application of stator torque and flux terms as control variables in DTC control. So, the performance of DPC schemes relies on two key factors which are the precise evaluation of the instantaneous active and reactive power values and the precise orientation of power-source voltage vector position [11] or virtual-flux vector position [12]. Further, the main idea of DPC is to select the best switching state of the power switches through a lookup table with hysteresis comparisons to achieve a unity power factor operation, and to maintain dc-link voltage constant [13]. Further, one feature of the traditional DPC scheme is the fast dynamic power regulation response. However, the main shortfalls of this DPC scheme are; to obtain satisfactory performance, it needs a higher sampling frequency, and a variable switching frequency. To defeat these shortfalls, many modified DPC schemes with a constant switching frequency, such as model predictive direct power control [14, 15], DPC based PI control [16], DPC slide-mode control [17], vector sequences with duty cycle calculating [18], have been extremely proposed and reported for power electronic systems in recent years.

In this paper, a nonlinear backstepping control method with predictive direct power control is proposed to control a photovoltaic system acting as a shunt active power filter (PV-SAPF). The essential function of the filtering system are reactive power compensation and harmonic currents reduction. Ideally, the presented system needs to generate enough reactive power and harmonic currents to compensate for the hurtful effect of nonlinear loads on the utility grid. Furthermore, to extract maximum quantity of power from the photovoltaic generator, a suitable backstepping current control method for the DC-DC boost converter is also developed.

Digital processor technology has been quickly developed in the past decades and has influenced many fields. Recently, increasingly processors, such as Digital Signal Processors (DSP), have been used to implement large, fast and complex digital control algorithms. The control dynamics sufficiently cannot often be captured by the traditional software-only simulation methodology. Methods to bridge the deficit between simulation and deployment can be Processor-in-the-Loop (PIL) methodology [19]. Furthermore, PIL procedure can provide important measurements on the software system such as memory usage and control algorithm execution. These data help designers to implement and test digital control systems and their hardware at the beginning of the whole design process, thus limiting the use of error-prone procedures [20]. For these reasons, the PIL has been increasingly used to co-simulate power converts. For instance, a DC-DC buck converter feeding a DC motor based on PIL approach was proposed in [21] . Three-phase power converter based on the processor in the loop was studied in [22] [6]. In the reference [23], a three-phase shunt active power filter implemented with processor in the loop was proposed.

In this paper, all the control algorithms for the presented control system are modelled in MATLAB/Simulink platform using embedded Matlab functions and transferred into C code, this last generated algorithm codes are embedded in a real target DSP (STM32F429i-Discovery). Moreover, the embedded DSP control algorithm controls the presented system (PV-SAPF) part modelled in the host PC represented by the Simulink platform.

This paper is organized as follows: in section II, description and modeling of the SAPF side system and DC-DC boost converter side are given. In section III, the control synthesis of the DC-DC boost converter is presented. In section IV, synthesis and design of the proposed controllers for the SAPF are developed. In section V, description of processor-in-the-loop prototype, and co-simulation results are given and discussed. Finally, the paper is concluded in its last section.

2. SYSTEM DESCRIPTION AND MODELING

2.1. System Description

The utility grid is supposed to be a sinusoidal voltage source with series short circuit impedances. The grid is modeled by three-phase electromotive forces in series with impedances as shown in Fig. 1. In the right side of the system, a nonlinear load is connected to the utility grid through intermediate line impedances (L_l, R_l). Moreover, this load is composed of uncontrolled three-phase rectifier supplying a load (R_d, L_d) in its DC side. In the same figure, a DC-DC boost converter is utilized to interface the photovoltaic generator with the grid across a Voltage Source Inverter (VSI). The inverter, connected in parallel at the Point of Common Coupling (PCC), acts, in the same time, as a PV inverter and SAPF where it is often controlled as a current generator. Hence, in order to make grid current pure sinusoidal, the active filter injects unbalanced currents equal and in phase opposition of those absorbed by the nonlinear load.

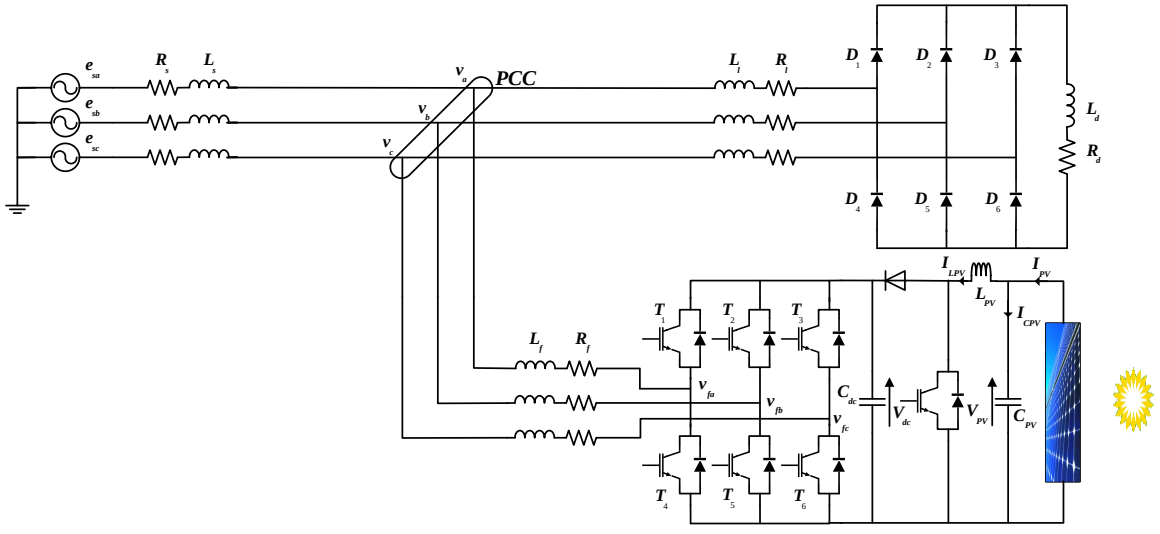

Fig. 1. Power circuit of grid-connected photovoltaic system acting as a shunt active power filter.

Briefly, the active filter function of the proposed system prevents disturbance currents generated by the nonlinear load to circulate through the grid impedances. Thus, the resulting total currents drawn from the AC main side are pure sinusoidal and balanced.

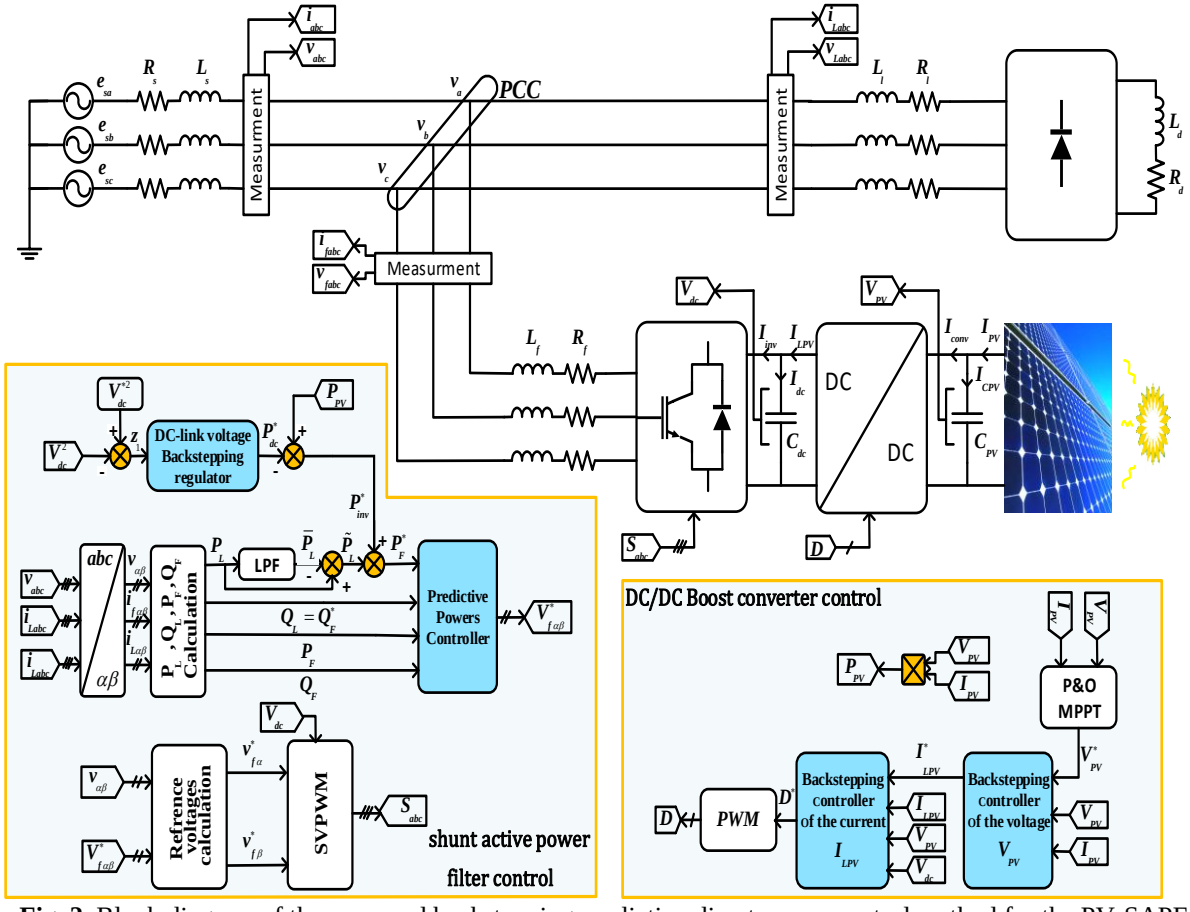

Fig. 2. Block diagram of the proposed backstepping predictive direct power control method for the PV-SAPF.

2.2. DC-DC Boost Converter Modeling and Control

2.2.1. DC-DC boost converter modeling

The DC-DC boost converter scheme is represented in Fig. 3. The dynamic equations (1) is presenting the state space model for this converter as follows:

$$\begin{aligned}\frac{dV_{PV}}{dt} &= \frac{1}{C_{PV}} I_{PV} - \frac{1}{C_{PV}} I_{LPV} \\ \frac{dI_{LPV}}{dt} &= \frac{1}{L_{PV}} V_{PV} - \frac{1}{L_{PV}} (1-D) V_{dc}\end{aligned} \quad (1)$$

2.2.2. Mathematical model of the SAPF side modeling

The system equations defining the SAPF in the three-phase reference frame are given by:

$$\begin{aligned}L_f \frac{di_{fa}}{dt} &= -R_f i_{fa} + v_{fa} - v_a \\ L_f \frac{di_{fb}}{dt} &= -R_f i_{fb} + v_{fb} - v_b \\ L_f \frac{di_{fc}}{dt} &= -R_f i_{fc} + v_{fc} - v_c \\ C_{dc} \frac{dV_{dc}}{dt} &= S_a i_{fa} + S_b i_{fb} + S_c i_{fc}\end{aligned} \quad (2)$$

Where, i_{fi}, v_{fi} with $i = a,b,c$ represent the AC side currents and voltages of the SAPF, respectively; v_i, $i = a,b,c$ are the point of common coupling voltages; L_f, R_f are the output inductance and resistance of the shunt active power filter, respectively; S_i, $i = a,b,c$ are the control signals for the VSI, V_{dc} is the voltage across the DC capacitor C_{dc}.

The mathematical model of SAPF in the stationary reference is given as follows:

$$\begin{aligned}L_f \frac{di_{f\alpha}}{dt} &= -R_f i_{f\alpha} + v_{f\alpha} - v_\alpha \\ L_f \frac{di_{f\beta}}{dt} &= -R_f i_{f\beta} + v_{f\beta} - v_\beta \\ C_{dc} \frac{dV_{dc}}{dt} &= \frac{P_{dc}}{V_{dc}}\end{aligned} \quad (3)$$

Where, i_{fi}, v_{fi} with $i = \alpha,\beta$ represent the AC side current and voltage components of the SAPF in the stationary reference, respectively, v_α, v_β are the point of common coupling voltages in the stationary reference, P_{dc} is the DC active power across the capacitor C_{dc}.

2.2.3. The New mathematical model of the SAPF for powers control

The powers at the output of the SAPF are given as:

$$\begin{bmatrix} P_F \\ Q_F \end{bmatrix} = \begin{bmatrix} v_\alpha & v_\beta \\ -v_\beta & v_\alpha \end{bmatrix} \begin{bmatrix} i_{f\alpha} \\ i_{f\beta} \end{bmatrix} \quad (4)$$

With a view to calculate the powers derivatives, the Lie derivative method is used; the active and reactive powers must be chosen as outputs. The two first equations of the system (3) can be written as follow:

$$\begin{aligned}\frac{dx}{dt} &= f(x) + g(x)u \\ y &= h(x)\end{aligned} \quad (5)$$

Where,

$$x = \begin{bmatrix} i_{f\alpha} \\ i_{f\beta} \end{bmatrix}, f(x) = \begin{bmatrix} f_1 \\ f_2 \end{bmatrix} = \frac{1}{L_f} \begin{bmatrix} -R_f i_{f\alpha} - v_\alpha \\ -R_f i_{f\beta} - v_\beta \end{bmatrix},$$
$$g(x) = \frac{1}{L_f} \begin{bmatrix} 1 & 0 \\ 0 & 1 \end{bmatrix}, u = \begin{bmatrix} v_{f\alpha} \\ v_{f\beta} \end{bmatrix}, y = \begin{bmatrix} h_1 \\ h_2 \end{bmatrix} = \begin{bmatrix} P_F \\ Q_F \end{bmatrix}$$

Where, $f(x)$ and $h(x)$ are a second order smooth vector fields, $g(x)$ is an 2×2 matrix of smooth vector field columns, u and y are 2×1 vectors of input and output respectively.

The derivative of each output can be expressed as follows [24]:

$$\frac{dy_i}{dx} = L_f h_i + L_g h_i u \quad (6)$$

Where, $L_f h_i$, $L_g h_i$ are the Lie derivatives of h_i with respect to f and g, respectively. The derivatives of powers are given as:

$$\begin{aligned}\frac{dP_F}{dt} &= v_\alpha f_1 + v_\beta f_2 + \frac{v_\alpha}{L_f} v_{f\alpha} + \frac{v_\beta}{L_f} v_{f\beta} \\ \frac{dQ_F}{dt} &= -v_\beta f_1 + v_\alpha f_2 - \frac{v_\beta}{L_f} v_{f\alpha} + \frac{v_\alpha}{L_f} v_{f\beta}\end{aligned} \quad (7)$$

After more simplification, the final new model of the SAPF is given as follows:

$$\begin{aligned}\frac{dP_F}{dt} &= \frac{1}{L_f}\left(-R_f P_F + V_{f\alpha}\right)\\ \frac{dQ_F}{dt} &= \frac{1}{L_f}\left(-R_f Q_F + V_{f\beta}\right)\\ \frac{dV_{dc}}{dt} &= \frac{P_{dc}}{V_{dc}C_{dc}}\end{aligned} \quad (8)$$

Where,

$$V_{f\alpha} = v_\alpha v_{f\alpha} + v_\beta v_{f\beta} - \left(v_\alpha^2 + v_\beta^2\right)$$
$$V_{f\beta} = -v_\beta v_{f\alpha} + v_\alpha v_{f\beta}$$

3. PV SIDE CONTROL

3.1. Backstepping control of DC-DC boost converter

The backstepping algorithm is based on the idea that specific variables can be utilized as virtual controls to make the original high order system simple. So, the final control outputs can be established step by step through suitable Lyapunov functions that guarantee the global stability [25]. On the contrary of other methods, the backstepping control method does not have constraints on the type of non-linearities, all control objectives are in fact achieved by using tools from the Lyapunov stability. This control method was successfully applied on a growing collection of plants [26].

To extract the maximum of power from the PV array, the backstepping control approach is proposed for the DC-DC boost converter. As shown in Fig. 3, to control the photovoltaic generator output voltage and current, two backstepping controllers are needed. The control method of the voltage is accomplished for the boost converter by controlling the voltage V_{pv} of the PV generator to its reference V_{pv}^{*} offered by Perturb and Observe (P&O) Maximum Power Point Tracking Algorithm (MPPT). The output of the voltage loop controller and the PV current compensation provides the current reference I_{Lpv}^{*} of the inner loop current controller. So, the duty cycle of the converter is provided by the current control loop and the PV voltage V_{pv} and V_{dc} compensations.

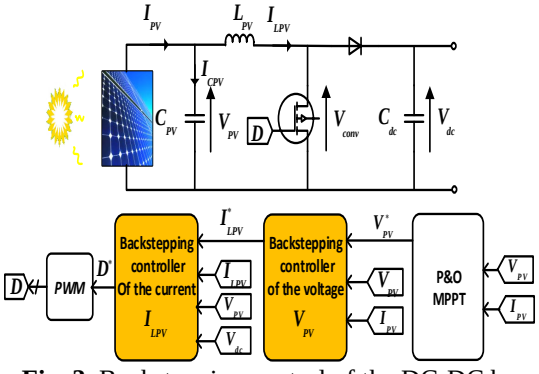

Fig. 3. Backstepping control of the DC-DC boost converter.

The needed backstepping controllers for the DC-DC boost converter are preformed based on a decomposition of the general model given by (1) into two subsystems, as follows:

Subsystem 1:

$$\frac{dV_{PV}}{dt} = \frac{1}{C_{PV}} I_{PV} - \frac{1}{C_{PV}} I_{LPV} \quad (9)$$

In this first subsystem, the PV output voltage V_{PV} is considered as an output variable while the current I_{LPV} is considered as a variable control.

Subsystem 2:

In the second subsystem described by the equation (10), the PV current I_{LPV} is considered as an output variable and the duty cycle D is considered as a variable control.

$$\frac{dI_{LPV}}{dt} = \frac{1}{L_{PV}} V_{PV} - \frac{1}{L_{PV}}\left(1 - D\right) V_{dc} \quad (10)$$

3.1.1. PV voltage backstepping controller synthesis

The desired backstepping regulator of the voltage V_{PV} synthesis is based on the first subsystem, defined by the equation (9), and analyzed as follows:

The variable error z_{Vpv} is defined by:

$$z_{Vpv} = V_{PV}^{*} - V_{PV} \quad (11)$$

The error z_{Vpv} dynamics is given by:

$$\frac{dz_{Vpv}}{dt}=\frac{dV^{*}_{PV}}{dt}-\left(\frac{1}{C_{PV}}I_{PV}-\frac{1}{C_{PV}}I^{*}_{LPV}\right) \quad (12)$$

The candidate function of Lyapunov is chosen as:

$$V_{Vpv}=\frac{1}{2}z^{2}_{Vpv} \quad (13)$$

The function (13) derivative is given as:

$$\frac{dV_{Vpv}}{dt}=z_{Vpv}\left(\frac{dV^{*}_{PV}}{dt}-\left(\frac{1}{C_{PV}}I_{PV}-\frac{1}{C_{PV}}I^{*}_{LPV}\right)\right) \quad (14)$$

When the derivative of the Lyapunov function is negative, the stability of the system is guaranteed; that can be achieved by choosing the derivative of z_{Vpv} as:

$$\frac{dz_{Vpv}}{dt}=-k_{Vpv}z_{Vpv} \quad (15)$$

Where, k_{Vpv} is a positive constant.

So, the reference current I^{*}_{LPV} is calculated as given in equation (16) and the Fig. 4 represents its controller block diagram.

$$I^{*}_{LPV}=-I_{PV}-k_{Vpv}C_{PV}\left(V^{*}_{PV}-V_{PV}\right)+C_{PV}\frac{dV^{*}_{PV}}{dt} \quad (16)$$

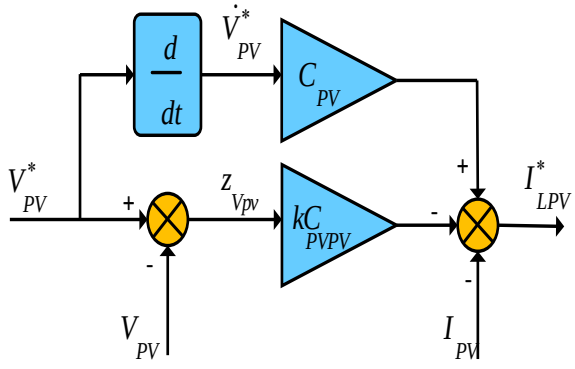

Fig. 4. Backstepping controller block diagram of the PV output voltage.

3.1.2. PV current backstepping controller synthesis

The desired backstepping regulator of the current I_{LPV} synthesis is based on the second subsystem, defined by the equation (10), which is analyzed as follows:

The definition of the variable error z_{ILpv} is given by:

$$z_{ILpv}=I^{*}_{LPV}-I_{LPV} \quad (17)$$

The error z_{ILpv} dynamics is given by:

$$\frac{dz_{ILpv}}{dt}=\frac{dI^{*}_{PV}}{dt}-\left(\frac{1}{L_{PV}}V_{PV}-\frac{1}{L_{PV}}\left(1-D^{*}\right)V_{dc}\right) \quad (18)$$

The candidate function of Lyapunov is chosen as:

$$V_{ILpv}=\frac{1}{2}z^{2}_{ILpv} \quad (19)$$

The function (19) derivative of is:

$$\frac{dV_{2}}{dt}=z_{ILpv}\left(\frac{dI^{*}_{PV}}{dt}-\left(\frac{1}{L_{PV}}V_{PV}-\frac{1}{L_{PV}}\left(1-D^{*}\right)V_{dc}\right)\right) \quad (20)$$

The system stability is ensured by choosing the derivative of z_{ILpv} as:

$$\frac{dz_{ILpv}}{dt}=-k_{ILpv}z_{ILpv} \quad (21)$$

Where, k_{ILpv} is a positive constant.

Hence, the reference of duty cycle D^{*} is calculated as given by the equation (22), and Fig. 5 presented its controller block diagram.

$$D^{*}=\frac{1}{V_{dc}}\left(L_{PV}\frac{dI^{*}_{LPV}}{dt}-V_{PV}+V_{dc}+L_{PV}k_{ILpv}\left(I^{*}_{LPV}-I_{LPV}\right)\right) \quad (22)$$

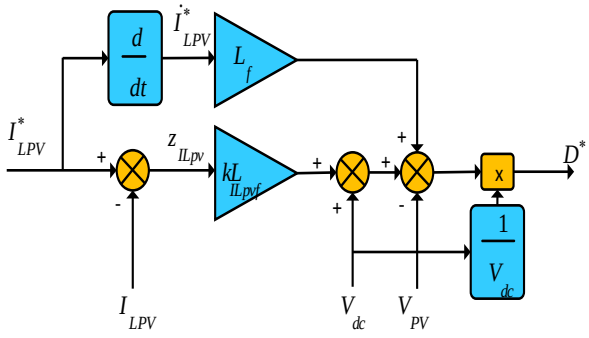

Fig. 5. Backstepping controller block diagram of the PV current.

4. SAPF SIDE CONTROL STRATEGY

The actual capacitor square voltage V_{dc}^2 is compared with its reference square value V_{dc}^{*2} as shown in Fig. 2; the error between the capacitor voltage and its reference is fed to a nonlinear controller. The active power reference P_{dc}^* across the capacitor C_{dc} presents the output of the nonlinear voltage controller. Moreover, the compensating powers are calculated based on the instantaneous p–q theory, using 4-order Low-Pass Filter (LPF), the average powers are extracted. Further, the oscillating powers are obtained through a simple subtraction of the average power from the active and reactive powers.

4.1. p–q Theory based Control Strategy

The nonlinear load instantaneous active and reactive powers are calculated as follows:

$$\begin{bmatrix} P_L \\ Q_L \end{bmatrix} = \begin{bmatrix} v_\alpha & v_\beta \\ -v_\beta & v_\alpha \end{bmatrix} \begin{bmatrix} i_{L\alpha} \\ i_{L\beta} \end{bmatrix} \tag{23}$$

The instantaneous active and reactive powers, including average and oscillating values, are expressed as follows:

$$\begin{aligned} P_L &= \bar{P}_L + \tilde{P}_L \\ Q_L &= \bar{Q}_L + \tilde{Q}_L \end{aligned} \tag{24}$$

The average values ($\bar{P}_L$, $\bar{Q}_L$) are representing the average active power and reactive power produced from the nonlinear load current positive-sequence component. ($\tilde{P}_L$, $\tilde{Q}_L$) are the ripple active and reactive powers of the oscillating values of P_L and Q_L [27]. Moreover, for harmonics and reactive power compensation, balancing of the three-phase unbalanced load currents, all of the harmonic component value $\tilde{P}_L$ of the active power and the reactive power value Q_L are chosen as compensation reference of power as follows:

$$\begin{aligned} P_F^* &= \bar{P}_L - P_{dc}^* + P_{PV} \\ Q_F^* &= Q_L \end{aligned} \tag{25}$$

The DC-link capacitor P_{dc}^* power reference is used as an average real power and is obtained from the nonlinear backstepping DC voltage controller, and the power P_{PV} is the active power delivered from the photovoltaic generator used as a compensating power, (P_F, Q_F) are the active and reactive filter powers, respectively.

4.2. DC-link Voltage Backstepping Controller Synthesis

In the first subsystem described by the equation (8), the voltage V_{dc} is considered as an output variable while the instantaneous active power P_{dc}^* is considered as a control variable.

$$\frac{dV_{dc}}{dt} = \frac{P_{dc}}{V_{dc} C_{dc}} \tag{26}$$

To maintain the DC-link voltage across the capacitor C_{dc} at a constant desired reference value, a backstepping controller is used to maintain the DC-link voltage at its desired value covering the inverter losses. For forcing the DC-link voltage follow its reference, the tracking variable error z_1 is defined by:

$$z_1 = V_{dc}^* - V_{dc} \tag{27}$$

The error z_1 dynamics is given by:

$$\frac{dz_1}{dt} = \frac{dV_{dc}^*}{dt} - \frac{P_{dc}^*}{V_{dc} C_{dc}} \tag{28}$$

The Lyapunov candidate function is chosen as:

$$V_1 = \frac{1}{2} z_1^2 \tag{29}$$

The derivative of the function (29) is expressed as:

$$\frac{dV_1}{dt} = z_1\left(\frac{dV_{dc}^*}{dt} - \frac{P_{dc}^*}{V_{dc}C_{dc}}\right) \quad (30)$$

The stability of the system is ensured while the derivative of the Lyapunov function must be negative. Consequently, this can be achieved by choosing the derivative of z_1 as:

$$\frac{dz_1}{dt} = -k_1 z_1 \quad (31)$$

Where, k_1 is a positive gain.

Consequently, the control law of the DC-Link voltage is given by the equation (32) below and its controller block diagram is presented in Fig. 6.

$$P_{dc}^* = V_{dc}C_{dc}\left(\frac{dV_{dc}^*}{dt} + k_1 z_1\right) \quad (32)$$

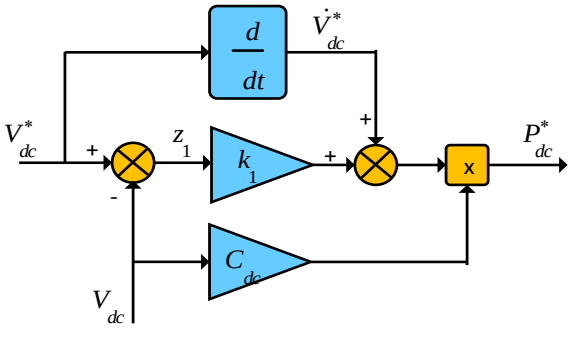

Fig. 6. Controller block diagram of the DC-link voltage backstepping controller.

4.3. Predictive Powers Controller Synthesis

The measures and commands of the active and reactive powers are used as input data variables of the presented predictive algorithm scheme as shown in Fig. 2. At each sampling period T_e of the process control beginning, for the cancellation of the active and reactive powers tracking errors at the end of this sampling period, the SAPF average voltage vectors $V_{F\alpha\beta}$ are calculated. So, to generate a sequence of switching states, SVPWM is used to accomplish the control strategy objective with a constant switching frequency. The Predictive Direct Power Control (PDPC) uses a nonlinear backstepping DC-link voltage controller to produce the reference of the DC power component P_{dc}^*. Consequently, the digital PDPC control law that gives the desired SAPF average voltage vector which will be applied during each sampling period T_e is given by the following steps:

If the sampling period T_e is infinitely small compared with the fundamental period, the discretization of the two first equations of (8) yields:

$$\begin{aligned} P_F(k+1) - P_F(k) &= \frac{T_e}{L_f}(-R_f P_F(k) + V_{F\alpha}(k)) \\ Q_F(k+1) - Q_F(k) &= \frac{T_e}{L_f}(-R_f Q_F(k) + V_{F\beta}(k)) \end{aligned} \quad (33)$$

The control objective is to force the active and reactive powers to track their reference values at the next sampling period, the equation (33) can be rewritten as follows:

$$\begin{aligned} P_F^*(k+1) = P_F(k+1) &= \frac{T_e}{L_f}(-R_f P_F(k) + V_{F\alpha}(k)) \\ Q_F^*(k+1) = Q_F(k+1) &= \frac{T_e}{L_f}(-R_f Q_F(k) + V_{F\beta}(k)) \end{aligned} \quad (34)$$

Using the equation (34), the required SAPF average voltage vector is expressed as follows:

$$\begin{aligned} V_{F\alpha}(k) &= R_f P_F(k) + \frac{L_f}{T_e}(P_F^*(k+1) - P_F(k)) \\ V_{F\beta}(k) &= R_f Q_F(k) + \frac{L_f}{T_e}(Q_F^*(k+1) - Q_F(k)) \end{aligned} \quad (35)$$

At the next sampling period (k+1), the instantaneous power references can be estimated using a linear extrapolation as shown in Fig. 7.

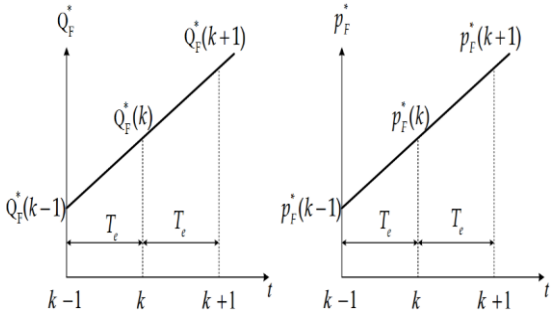

Fig. 7. Predictive value estimation of power references.

The estimated power references are given by:

$$P_F^*(k+1) = 2P_F^*(k) - P_F^*(k-1)$$
$$Q_F^*(k+1) = 2Q_F^*(k) - Q_F^*(k-1) \quad (36)$$

Consequently, the final digital PDPC control law which provides the required SAPF average voltage vector that is applied during each sampling period is given by the following equation:

$$V_{F\alpha}(k) = R_f P_F(k) + \frac{L_f}{T_e}(\Delta P_F^*(k) + e_{P_F}(k))$$
$$V_{F\beta}(k) = R_f Q_F(k) + \frac{L_f}{T_e}(\Delta Q_F^*(k) + e_{Q_F}(k)) \quad (37)$$

Where, $e_{P_F}(k)$ and $e_{Q_F}(k)$ are the actual active and reactive powers tracking errors defined as:

$$e_{P_F}(k) = P_F^*(k) - P_F(k)$$
$$e_{Q_F}(k) = Q_F^*(k) - Q_F(k) \quad (38)$$

$\Delta P_F^*(k)$ and $\Delta Q_F^*(k)$ are the actual change in active and reactive powers references given by:

$$\Delta P_F^*(k) = P_F^*(k) - P_F^*(k-1)$$
$$\Delta Q_F^*(k) = Q_F^*(k) - Q_F^*(k-1) \quad (39)$$

Once the intermediate voltage $V_{f\alpha}^*$ and $V_{f\beta}^*$ is obtained, the reference voltage $v_{f\alpha}^*$ and $v_{f\beta}^*$ can be calculated using (8) as follows:

$$v_{f\alpha}^* = \frac{v_\alpha}{v_\alpha^2 + v_\beta^2} V_{f\alpha}^* - \frac{v_\beta}{v_\alpha^2 + v_\beta^2} V_{f\beta}^* + v_\alpha \quad (40)$$

And,

$$v_{f\beta}^* = \frac{v_\beta}{v_\alpha^2 + v_\beta^2} V_{f\alpha}^* + \frac{v_\alpha}{v_\alpha^2 + v_\beta^2} V_{f\beta}^* + v_\beta \quad (41)$$

The digital predictive direct power control scheme provides the required shunt active power average voltage vectors that is applied during each sampling period, the reference voltage $v_{f\alpha}^*(k)$ and $v_{f\beta}^*(k)$ is presented in Fig. 8.

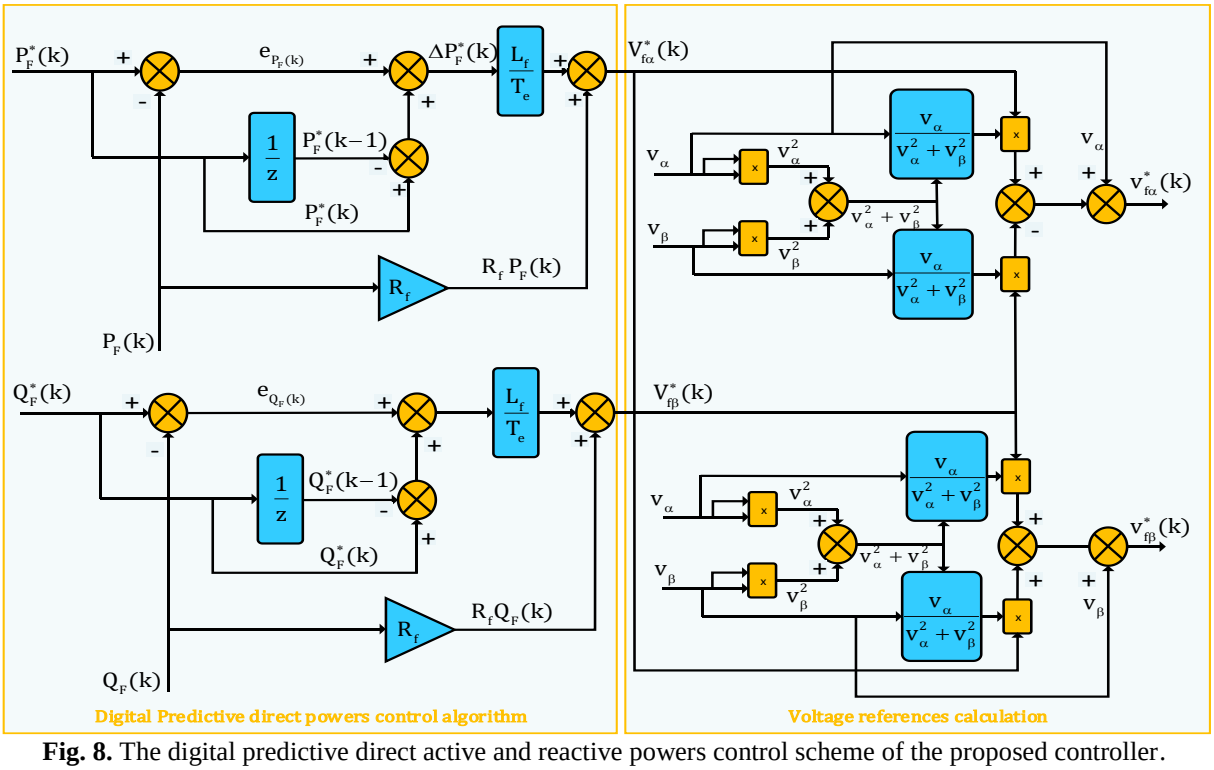

Fig. 8. The digital predictive direct active and reactive powers control scheme of the proposed controller.

5. PRINCIPLE OF PROTOTYPING PROCESSOR-IN-THE-LOOP

In PIL co-simulation, an embedded platform running the control algorithm is connected to a host standard computer in which the physical system model is executed. Thus, an appreciation regarding the execution circumstances of the developed algorithm can be accomplished aiming to optimize some important factors such as memory footprint, code size, and algorithm execution required time. The principle of the PIL based development is presented in Fig. 9.

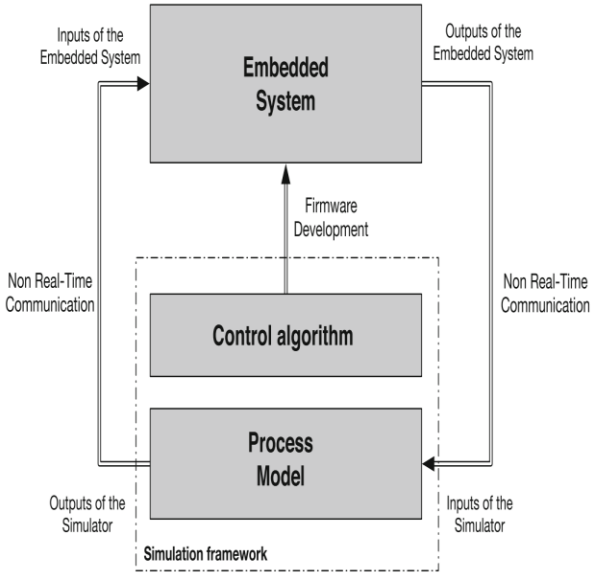

Fig. 9. Block diagram of embedded system connected to a PIL simulator.

The digital implementation of the control algorithms using a real DSP board is verified and validated through the PIL prototyping, and this is before embedding it into a real power environment. The interest of the PIL prototyping is permitted to validate the digital control algorithms implementation of a control part while simulating the power part by computer. Thereafter, it is possible to validate the control algorithms in a virtual environment where the control algorithms could be corrected and modified without costly hardware iteration. Moreover, this leads to decrease the cost of a project as well as the development time. So, it is possible to evaluate the performance of the system control algorithms and the its weak points can be discovered in this virtual environment while eliminating the risk of damaging all or part of the electrical system.

In order to implement the PIL co-simulation, a communication link has to be set up between the target and the host. In the given board of study, with standard communication protocol as defined by the manufacturer, UART (Universal Asynchronous Receiver Transmitter) communication is used. The port parameter settings are fixed from PC as defined by manufacturer and the application programming interface (API). Further, as STM DSP board has several serial communication options, a specific UART communication port can be set, which enables the embedded systems to send and receive the information to external devices. Fig. 10 shows the connection between the serial communication Transmit Data (Tx) pin of the transmitter with Received Data (Rx) pin of the receiver. Moreover, note that the receiver and the transmitter should have a common ground. In the given study, USB to RS232 TTL UART Prolific FTDI232 (serial communication) converter is used to communicate between the host PC and target board. The host, target device/board, and the communication link are shown in Fig. 10.

5.1. Co-simulation Results

To validate the proposed control method algorithms and estimate its performances, the system has been modeled using embedded MATLAB functions, and it is co-simulated through the processor-in-the-loop technique using STM32F429i-discovery DSP board. The co-simulation parameters of the proposed PV-SAPF and its control as well as those of the PV generator are collected in Tables 1 and 2, respectively. It is question also to exhibit the capability of the system to guarantee an active and reactive powers sharing between the shunt active power filter and distribution utility grid at the PCC under unexpected variations of load condition. Where at time t=0.15s another linear load is connected to PCC with the previous load, and is disconnected again at t=0.3s. Moreover, the system has been examined at the standard test conditions: constant irradiation of 1000 W/m² and a constant temperature of 25°. The results of the system behavior for proposed control method is given in the Figs. 11 to 13.

The source current before compensation and its harmonic spectrum are shown in Fig. 11; Fig. 11(a) shows an essential amount of harmonics in the source current with a Total Harmonic Distortion (THD) equal to 28.96% as shown in Fig. 11(b).

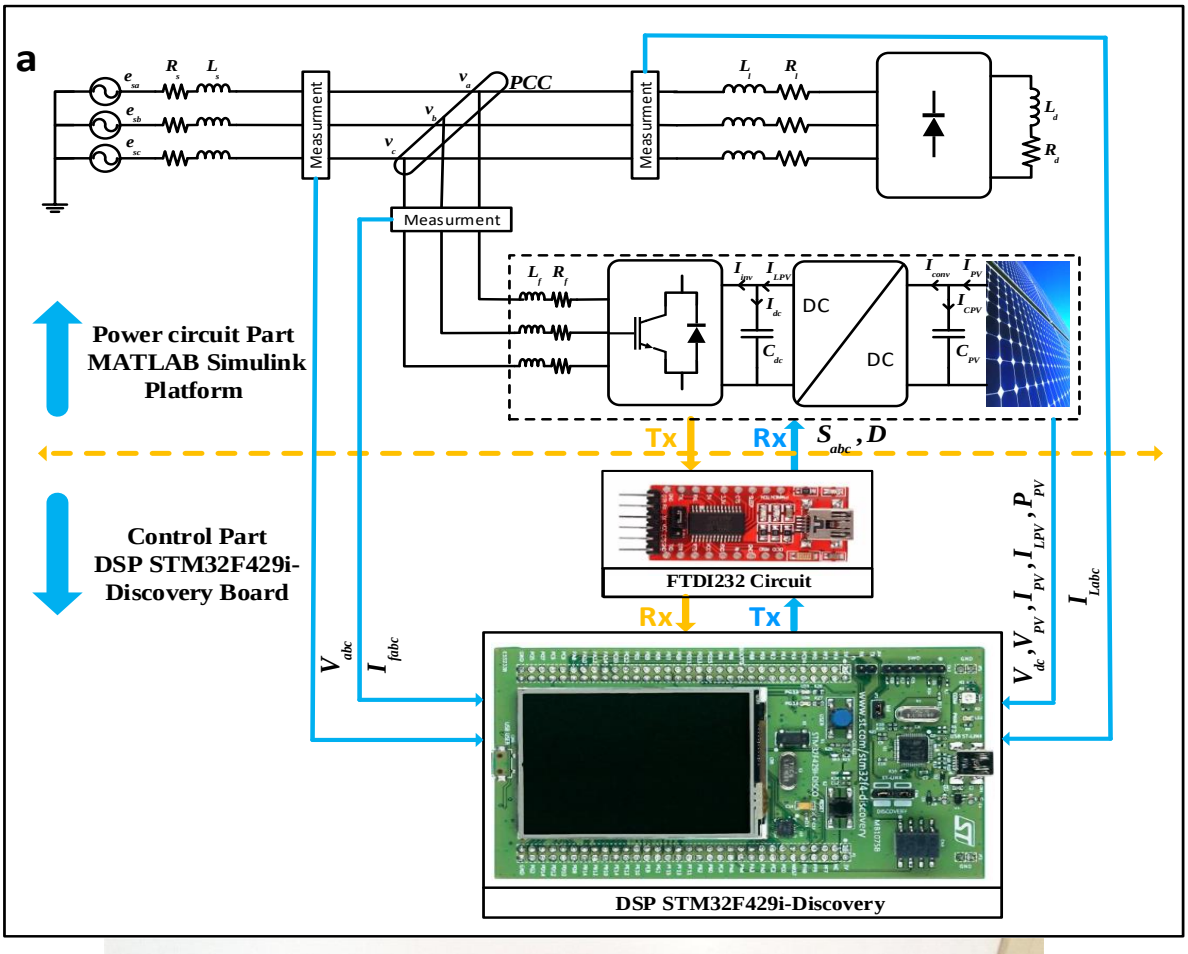

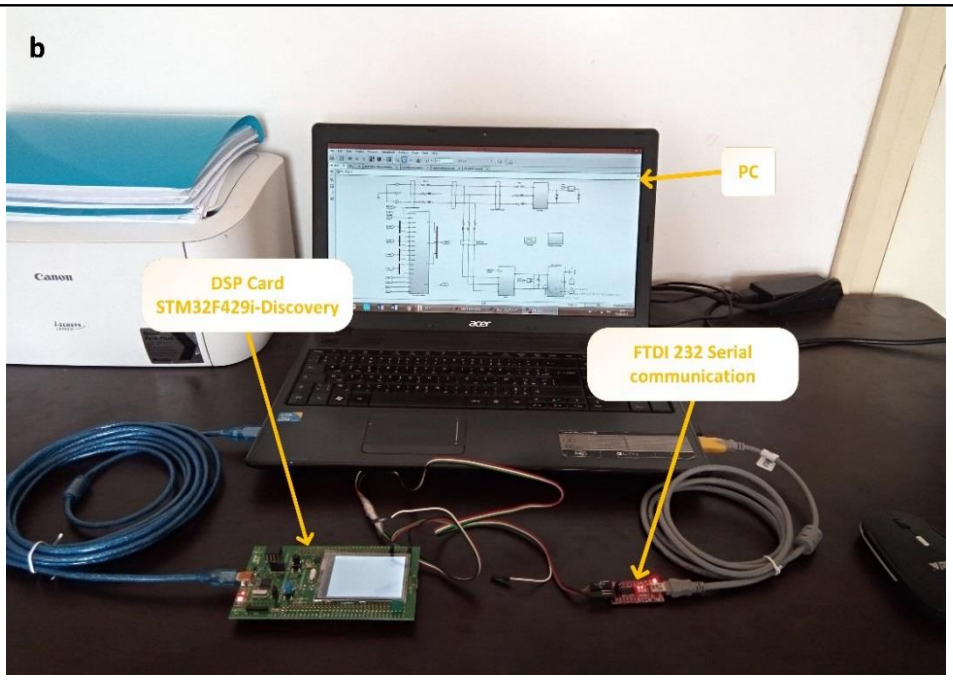

Fig. 10. Processor-in-the-loop technique: (a) host device/board, and communication link, (b) PIL co-simulation platform.

The dynamic responses of the PV-SAPF system controlled by proposed control approach during a sudden load variation are illustrated in Fig. 12. The waveforms include the injected filter current, three phase source currents, source voltage and current, source current harmonic spectrum, and DC-link capacitor voltage. In this test, another linear load with the same value as the first one is connected to the PCC at t=0.15s and it is disconnected again after 0.15s. From Fig. 12(b), the source current is sinusoidal and in phase with its corresponding voltage even during the step change caused by the added extra load as shown in the same figure. The THD of the source current is reduced from 28.96 % before compensation to 1.59 % after compensation as shown in Fig. 12(e). Hence, the source current is almost free of harmonic reactive current components, which leads to a unity power factor operation. Consequently, the results prove the efficiency and the effectiveness of the proposed predictive direct power control.

In Fig. 12(d), the DC-link voltage across the capacitor is managed constant during the load change with a drop voltage lower than 30 V; the recovery time is about 0.025s. Thus, this result confirms the efficiency of the DC-link voltage backstepping control.

The waveforms of the corresponding exchanged active and reactive powers between load, grid, and shunt active power filter are shown in Fig. 13, for the proposed control method. Fig. 13(a) shows that the active power of the shunt active power filter is added to the grid power with a view to supply the load active power demand. Moreover, the reactive powers waveforms, shown in Fig. 13(b) argue that the shunt active power filter accomplishes the load reactive power demand. This is demonstrated by a zero value of the grid reactive power. Fig. 13(c) shows the active power produced by the PV system, which is clearly equal to the maximum power of PV generator at the standard conditions. Further, the time response of the generated PV active power is about 0.005s for the proposed control method. The error between the generated PV power and its reference in steady state is about 50W. accordingly, these results confirm again the efficiency of the DC-DC boost converter backstepping controller.

Table 1. PV-SAPF system parameters.

SAPF side	
RMS value of phase voltage	220 V
DC-link capacitor C_{dc}	5 mF
Source impedance R_s, L_s	1.6 mΩ, 100 μH
Filter impedance R_f, L_f	1 mΩ, 350 μH
Line impedance R_l, L_l	2.7 mΩ, 25 μH
Diode rectifier load R_d, L_d	5 mΩ, 2.6 μH
Fundamental frequency f_s	50 H
DC-link voltage reference V_{dc}^*	700 V
Control constants parameters $k_1, k_2 = k_3$	170, 5×10^9
PV side system parameters	
Inductance L_{PV}	5 mH
Capacitance C_{PV}	55 mF
Control constants parameters k_{Vpv}, k_{ILpv}	13×10^6, 5×10^3

Table 2. The array parameters of the (BP Solar's SX 150 solar array) at the standard conditions.

Maximum power (P_{Max} **)**	**150 W**
Voltage at P_{Max} **(** V_{mp} **)**	34.5 V
Current at P_{Max} **(** I_{mp} **)**	4.35 A
Warranted minimum P_{Max}	140 W
Short-circuit current (I_{sc} **)**	4.75 A
Open-circuit voltage (V_{oc} **)**	43.5 V
Maximum system voltage	600 V
Temperature coefficient of I_{sc}	(0.065 ± 0.015)%/C°
Temperature coefficient of V_{oc}	$-(160 \pm 20)$mV/C°
Temperature coefficient of power	$-(0.5 \pm 0.05)$%/C°
NOCT	47 ± 2 C°

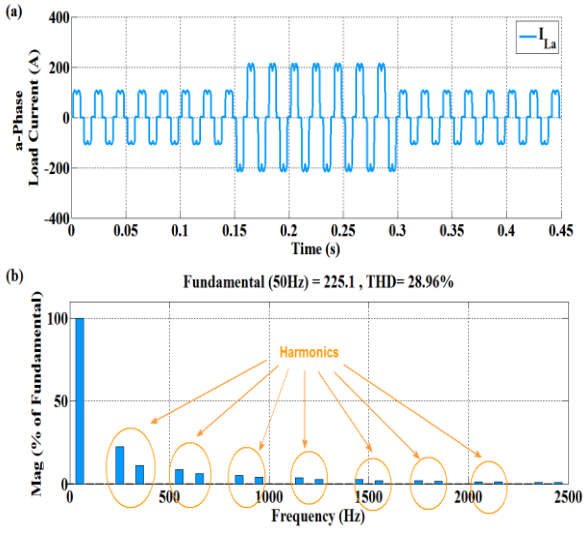

Fig. 11. PV-SAPF system responses without filtering function: (a) supply current before harmonics compensation in steady state, (b) harmonic spectrum of supply current.

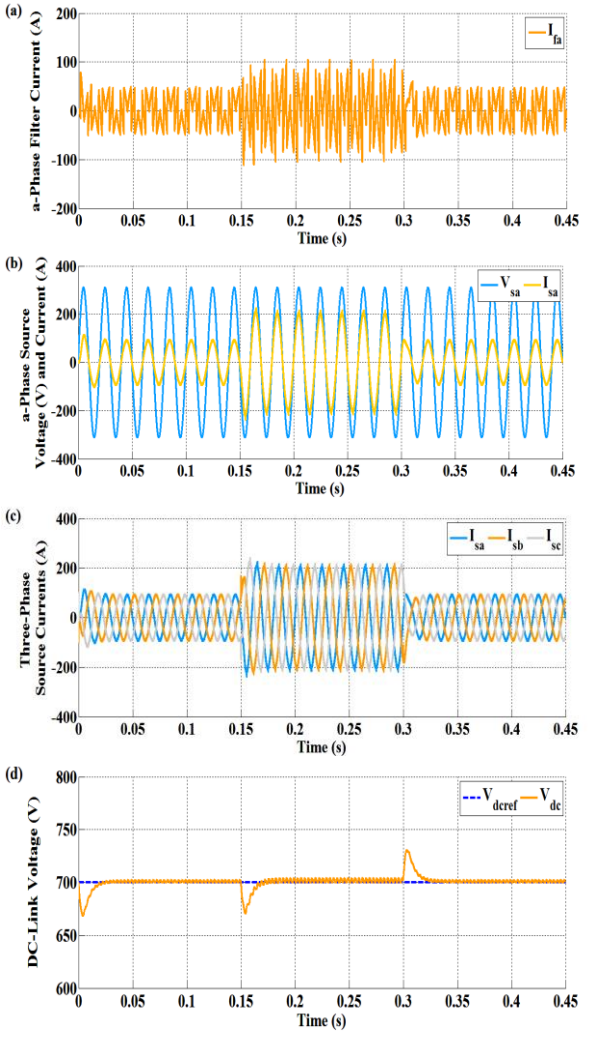

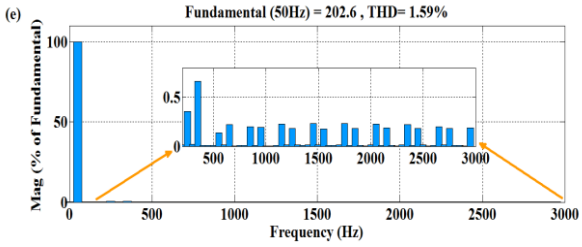

Fig. 12. Dynamic responses of the PV-SAPF system controlled by backstepping predictive direct power control: (a) filter current, (b) a-phase source voltage and source current, (c) three-phase source currents, (d) DC-link voltage, (e) harmonic spectrum of the line current.

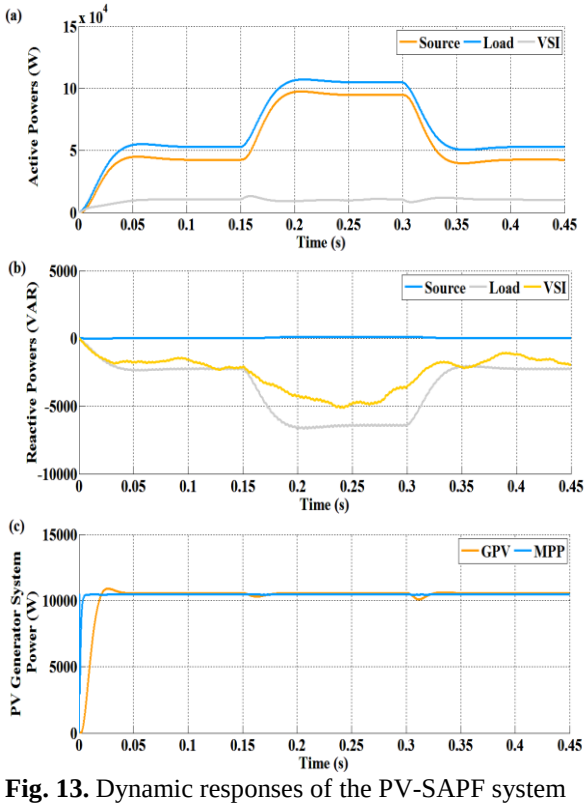

Fig. 13. Dynamic responses of the PV-SAPF system controlled by backstepping control: (a) grid, load, and voltage source inverter active powers, (b) grid, load, and voltage source inverter reactive powers, (c) power generated by the PV generator (GPV), maximum power point of PVG (MPP).

6. CONCLUSION

This paper has carried out a backstepping predictive direct power control for grid connected photovoltaic system acting as a shunt active power filter. Hence, the proposed control is intended to cancel the source current harmonics, reactive power compensation, DC-link voltage regulation, and transferring the optimal power from photovoltaic

generator into the utility grid. The PIL co-simulation combined with Matlab/Simulink are performed to show the usefulness of the proposed method, accordingly, the results of the proposed control method have reduced the harmonics and provides reactive power compensation due to non-linear load and sudden variations of this last. As a result, the source currents become sinusoidal, thus unity power factor operation and good power sharing performances between the PV generator and the utility grid are achieved.

REFERENCES

[1] A. El Fadili, F. Giri, and A. El Magri, **"Reference Voltage Optimizer for Maximum Power Point Tracking in Triphase Grid-Connected Photovoltaic Systems,"** *International Journal of Electrical Power & Energy Systems*, Vol. 60, pp. 293-301, 2014.

[2] K. Tsang and W. Chan, **"Three-level Grid-Connected Photovoltaic Inverter with Maximum Power Point Tracking,"** *Energy Conversion and management*, Vol. 65, pp. 221-227, 2013.

[3] M. Benadja, S. Saad, and A. Belhamra, **"Rapid Transaction to Load Variations of Active Filter Supplied by PV System,"** *Frontiers in Energy*, Vol. 8, pp. 335-344, 2014.

[4] P. Anjana, V. Gupta, H. Tiwari, and N. Gupta, **"PV Source Integrated Micro-grid for Power Quality Improvement,"** in *Transmission and Distribution Conference and Exposition (T&D), 2016 IEEE/PES*, pp. 1-5, 2016.

[5] R. Noroozian and G. B. Gharehpetian, **"An Investigation on Combined Operation of Active Power Filter with Photovoltaic Arrays,"** *International Journal of Electrical Power & Energy Systems*, Vol. 46, pp. 392-399, 2013.

[6] E. Romero-Cadaval, G. Spagnuolo, L. G. Franquelo, C. A. Ramos-Paja, T. Suntio, and W. M. Xiao, **"Grid-connected Photovoltaic Generation Plants: Components and Operation,"** *IEEE Industrial Electronics Magazine*, Vol. 7, pp. 6-20, 2013.

[7] J. Urbanetz, P. Braun, and R. Rüther, **"Power Quality Analysis of Grid-Connected Solar Photovoltaic Generators in Brazil,"** *Energy Conversion and management*, Vol. 64, pp. 8-14, 2012.

[8] M. A. Mahmud, H. Pota, and M. Hossain, **"Dynamic Stability of three-Phase Grid-Connected Photovoltaic System using Zero Dynamic Design Approach,"** *IEEE Journal of Photovoltaics*, Vol. 2, pp. 564-571, 2012.

[9] H. Akagi, Y. Kanazawa, and A. Nabae, **"Instantaneous Reactive Power Compensators Comprising Switching Devices Without Energy Storage Components,"** *IEEE Transactions on industry applications*, pp. 625-630, 1984.

[10] B. S. Chen and G. Joós, **"Direct Power Control Of Active Filters With Averaged Switching frequency Regulation,"** *IEEE Transactions on Power Electronics*, Vol. 23, pp. 2729-2737, 2008.

[11] T. Noguchi, H. Tomiki, S. Kondo, and I. Takahashi, **"Direct Power Control of PWM Converter Without Power-Source Voltage Sensors,"** *IEEE Transactions on Industry Applications*, Vol. 34, pp. 473-479, 1998.

[12] M. Malinowski, M. P. Kazmierkowski, S. Hansen, F. Blaabjerg, and G. Marques, **"Virtual-Flux-Based Direct Power Control of Three-phase PWM Rectifiers,"** *IEEE Transactions on industry applications*, Vol. 37, pp. 1019-1027, 2001.

[13] Y. Zhang, J. Long, Y. Zhang, T. Lu, Z. Zhao, and L. Jin, **"Table-based Direct Power Control for Three-Level Neutral Point-Clamped Pulse-Width Modulated Rectifier,"** *IET Power Electronics*, Vol. 6, pp. 1555-1562, 2013.

[14] R. Portillo, S. Vazquez, J. I. Leon, M. M. Prats, and L. G. Franquelo, **"Model based Adaptive Direct Power Control for Three-Level NPC Converters,"** *IEEE Transactions on Industrial Informatics*, Vol. 9, pp. 1148-1157, 2013.

[15] Y. Zhang, W. Xie, Z. Li, and Y. Zhang, **"Model Predictive Direct Power Control of a PWM Rectifier with Duty Cycle Optimization,"** *IEEE transactions on power electronics*, Vol. 28, pp. 5343-5351, 2013.

[16] P. R. Martinez-Rodriguez, G. Escobar, A. A. Valdez-Fernandez, M. Hernandez-Gomez, and J. M. Sosa, **"Direct Power Control of a Three-Phase Rectifier based on Positive Sequence Detection,"** *IEEE Transactions on Industrial Electronics*, Vol. 61, pp. 4084-4092, 2014.

[17] J. Hu, L. Shang, Y. He, and Z. Zhu, **"Direct Active and Reactive Power Regulation of Grid-Connected DC/AC Converters using Sliding Mode Control Approach,"** *IEEE transactions on power electronics*, Vol. 26, pp. 210-222, 2011.

[18] J. Hu and Z. Zhu, **"Improved Voltage-Vector Sequences on Dead-Beat Predictive Direct Power Control of Reversible Three-Phase Grid-Connected Voltage-Source Converters,"** *IEEE Transactions on Power Electronics*, Vol. 28, pp. 254-267, 2013.

[19] R. Liu, A. Monti, G. Francis, R. Burgos, F. Wang, and D. Boroyevich, **"Implementing a Processor-in-the-loop with a Universal Controller in the Virtual Test Bed,"** in *Power Electronics Specialists Conference, 2007. PESC 2007. IEEE*, Orlando, FL, USA, pp. 945-950, 2007.

[20] Z. Jiang, R. A. Dougal, R. Leonard, H. Figueroa, and A. Monti, **"Hardware-in-the-Loop Testing of Digital Power Controllers,"** in *Applied Power Electronics Conference and Exposition, 2006. APEC'06. Twenty-First Annual IEEE*, p. 6, 2006.

[21] J. Mina, Z. Flores, E. López, A. Pérez, and J.-H. Calleja, **"Processor-in-the-Loop and Hardware-in-the-loop Simulation of Electric Systems based in FPGA,"** in *Power Electronics (CIEP), 2016 13th International Conference on*, pp. 172-177, 2016.

[22] G. Francis, R. Burgos, P. Rodriguez, F. Wang, D. Boroyevich, R. Liu, *et al.*, **"Virtual Prototyping of Universal Control Architecture Systems by means of Processor in the Loop Technology,"** in *Applied Power Electronics Conference, APEC 2007-Twenty Second Annual IEEE*, pp. 21-27, 2007.

[23] G. W. Chang, R. C. Hong, and H. J. Su, **"An Efficient Reference Compensation Current Strategy of Three-Phase Shunt Active Power Filter Implemented with Processor-in-the-loop Simulation,"** *International Transactions on Electrical Energy Systems*, Vol. 24, pp. 125-140, 2014.

[24] C. Byrnes and A. Isidori, **"Output Regulation for Nonlinear Systems: an Overview,"** *International journal of robust and nonlinear control*, Vol. 10, pp. 323-337, 2000.

[25] M. Bouzidi, A. Benaissa, S. Barkat, S. Bouafia, and A. Bouzidi, **"Virtual Flux Direct Power Control of the Three-Level NPC Shunt Active Power Filter based on Backstepping Control,"** *International Journal of System Assurance Engineering and Management*, Vol. 8, pp. 287-300, 2017.

[26] Y. Zhang, B. Fidan, and P. A. Ioannou, **"Backstepping Control of Linear Time-Varying Systems With Known and Unknown Parameters,"** *IEEE Transactions on Automatic Control*, Vol. 48, pp. 1908-1925, 2003.

[27] E. H. Watanabe, H. Akagi, and M. Aredes, **"Instantaneous pq Power Theory for Compensating Nonsinusoidal Systems,"** in *Nonsinusoidal Currents and Compensation, 2008. ISNCC 2008. International School on*, pp. 1-10, 2008.